Article

Physicochemical Properties of a Bi-aromatic Heterocyclic-Azo/BSA Hybrid System at the Air−Water Interface

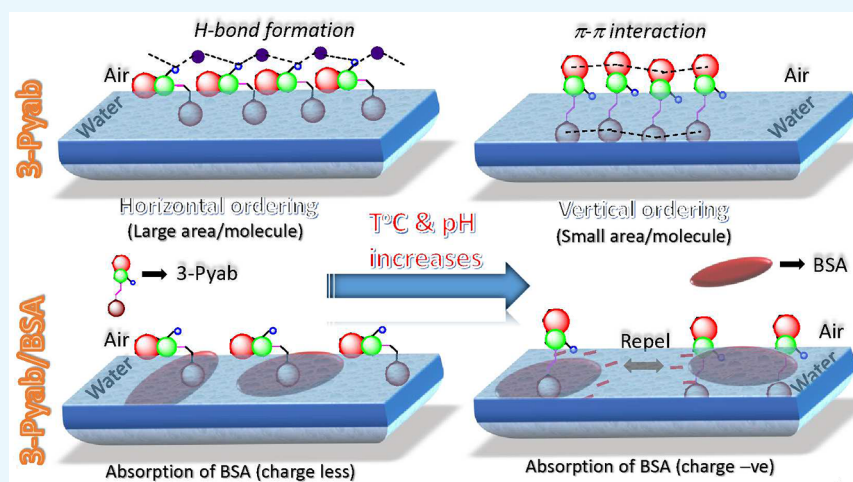Jayanta Kumar Bal,* Nilanjan Das, Tanmay Mathur, Jasper R. Plaisier, and Sabu Thomas

Read Online

ACCESS | Metrics & More | Article Recommendations | Supporting Information

ABSTRACT: The interaction of a heterocyclic azo compound with itself and with bovine serum albumin (BSA) is realized by probing the structural modifications in Langmuir (L) monolayers and Langmuir−Blodgett (LB) films. It was found from the pressure−area/molecule isotherms that the elastic, thermodynamic, and hysteretic properties of the pure azo L monolayer were strongly altered due to the variation of temperature and pH of subphase water. In addition to that, the modification of such properties of the azo L monolayer due to mixing with BSA was also studied. The incorporation of BSA within the azo molecular assembly reduced the elasticity of that assembly. Such reduction of in-plane elasticity of the pure azo monolayer can also be achieved by reducing the temperature and pH of subphase water without adding BSA. A reduction in area per molecule of the azo assembly at the air−water interface associated with the conformational change from horizontal to vertical orientation facilitating $\pi-\pi$ interaction was observed with increase in temperature and pH of the subphase. Such parameters also affected the interactions between azo and BSA molecules within the azo/BSA binary system. The structures of pure azo and binary films can be determined after they are transferred to hydrophilic and hydrophobic Si surfaces using the LB technique. Their out-of-plane and in-plane structures, as extracted from two complementary surface sensitive techniques, X-ray reflectivity and atomic force microscopy, were found to be strongly dependent on mixing with BSA, subphase pH, temperature, and substrate nature.

INTRODUCTION

N-Heterocyclic back bones are found in imidazole, pyridine, and benzimidazole derivatives, which are actively used in pharmaceutical fields.[1−5] N-Heterocyclic compound polarizability favors their solubility in many polar synthetic and natural solvents.[6,7] The majority of N-heterocyclic compounds having different physical properties are soluble in water.[8−10] Moderate solubility of benzimidazole in water allows its use in synthesis of useful drugs. Azo-heterocyclic compounds have been tremendously developed in the last few decades having valuable activity in biological fields.[11−13] But the amount of literature on mixed N-heterocyclic azo compounds is limited in literature.[14−16] In these azo-biheterocyclic compounds, the presence of a −N═N−C═N- azo−imine, functional group

between two N-heterocyclic substances promotes their activity.[17,18] Azo-benzimidazole compounds are of significant importance due to their use as potent antibacterial, antitubercular, antitumor, and antifungal substances.[19,20] Azo-benzimidazole also shows some particular physical properties, such as nonlinear optical and thermal properties.[21,22] The

presence of active N-hydrogen in the imidazole part of benzimidazole leads to a tendency to form H-bonds with several amino acids of different protein moieties. In contrast, one benzene ring fused within the imidazole (i.e., benzimidazole) decreases the solubility in hydrophilic solvent compare to the imidazole derivatives.[23−25] Essentially, one of these N-heterocyclic azo-imidazole compounds can exhibit many biological[26−30] and physical properties.[31,32]

The constituent nucleic acid bases of human cells are nothing but N-heterocyclic compounds that have an exocyclic −NH bond. Therefore, this azo compound might have potential interaction ability with other biomolecules. Thus, understanding the interactions between such technologically important azo compounds and biomolecules, such as bovine serum albumin (BSA), is of paramount importance for living organisms. BSA is an immune system protein. In the presence of foreign particles (antigens), it can help to create an antibody that protects the living systems. BSA is a potential colloidal delivery system since it is biodegradable, biocompatible, nontoxic, and nonimmunogenic.[33−37] Therefore, biologically active compounds can be carried by BSA and delivered to a target point in living systems.[38] We want to focus on the structural and physical property modification of an azo film due to the changes in pH and temperature of its surrounding medium. In addition, we want to shed light on how BSA modulates those physical properties and the structure of azo films at air−water (Langmuir monolayer) and air−solid (Langmuir−Blodgett film) interfaces as a function of pH and temperature of the medium. In this connection, we are trying to develop a new molecular level interactive path for the reaction between BSA and the reported azo compound. Various living things maintain a definite pH in their corresponding body circulation system. Hence, such studies at different pH values can be helpful for considering the application of azo molecules and BSA in living systems. Similarly, temperature is also a cofactor for interaction studies in living systems. The pharmacophore interacting ability of benzimidazole is present in biheterocyclic azo substances where the azo pyridine group actively participates supporting the ability to interact with BSA at air−water interfaces. Owing to the pharmaceutical properties of benzimidazole derivatives, designing an interaction study with BSA leads to one step forward toward their application in pharmaceutical fields. BSA interaction studies with pyridyl-azo-benzimidazole at the air−water interface via formation of Langmuir (L) and Langmuir−Blodgett (LB) films by changing the temperature and pH of the medium can establish a fundamental path for drug discovery. We are trying to explore the molecular level interaction between azo and BSA molecules in a LB trough. The LB technique provides an easy platform to investigate the mutual interaction mechanism between biomolecules under the desired environmental conditions (pH, temperature) of our interest.

In the present study, L films of pure azo and azo/BSA binary systems were monitored via pressure−area isotherm study followed by their structural characterization using X-ray reflectivity (XRR) and atomic force microscopy (AFM) techniques after transferring then onto Si surfaces. Based on a previous report,[16] we believe that the pyridyl-azo-benzimidazole could act as an antigen and could form antibodies by interacting with the BSA molecules. Therefore, the present study reporting various properties of such materials can create one step forward for future development of drug candidates.

■ EXPERIMENTAL SECTION

The meticulous synthesis route of 2-[(3′-pyridyl)azo]-benzimidazole (M_w = 223 g/mol) is elaborated elsewhere.[16] Orange colored diazonium salt solution of 3-aminopyridine was obtained by the reaction of 3-aminopyridine (184 mg) with $NaNO_2$ (138 mg) and concentrated H_2SO_4 (0.83 cm^3/5 cm^3; v/v) below 0 °C. Next, this solution was slowly added into an alkaline solution (KOH; 210 mg, Merck, purity 84%) of benzimidazole (236 mg, Sigma-Aldrich, purity 98%) while shaking and after complete addition of diazonium salt solution, a crude red-colored gummy precipitation was obtained. This crude product was carefully washed with distilled water. Pure 2-[(3′-pyridyl)azo]benzimidazole [labeled as 3-Pyab] was subsequently isolated by applying TLC and column chromatography. This newly synthesized compound was characterized by the analysis of different spectroscopic results.

For the preparation of films, Si(100) substrates (Sigma-Aldrich) were cleaned by RCA-treatment (Radio Corporation of America). The details of RCA cleaning were described elsewhere.[39] In RCA cleaning, the Si surfaces (size ∼25 × 15 mm^2) were made hydrophilic by introducing hydroxyl groups (−OH) after boiling them in a mixture of ammonium hydroxide (NH_4OH, Sigma-Aldrich, 25%), hydrogen peroxide (H_2O_2, Acros Organics, 39%), and Milli-Q water (H_2O/NH_4OH/H_2O_2 = 2:1:1, by volume) for 10 min at 100 °C. Some of the RCA-cleaned hydrophilic substrates were made hydrophobic by hydrofluoric acid (HF) treatment. Here, the RCA-cleaned Si were vertically immersed into HF (10%, 20 mL) solution for 3 min, and afterward the substrates were washed in Milli-Q water and dried prior to film deposition. The typical roughness of the RCA- and HF-treated Si varied between 4 and 8 Å. The quality of hydrophilicity and hydrophobicity was tested by water contact angle measurements, which yielded ∼14° and 79°, respectively.[40]

L and LB films were fabricated with a LB trough (Apex Instruments, model no. LBXD-NT) of inner working area 560 mm (length) × 200 mm (width) × 5 mm (height), kept in a clean environment. The LB trough was made of a polytetrafluoroethylene (PTFE) trough with two barriers moving toward each other. In the middle of the trough a Wilhelmy plate (a cut filter paper having a dimension of 10 × 25 mm^2) was dipped into the aqueous phase to measure the change in surface tension manifested as surface pressure. The LB trough was thoroughly cleaned with acetone, water purified with a Milli-Q system (resistivity ≈ 18 MΩ cm), and then ethanol followed by purified water for making the trough absolutely dust-free. The purity of the trough was examined by compressing the barrier over a pure water surface before spreading any molecules. If there was any impurity on the water surface, then pressure would rise upon compression. If this is the case, then further cleaning is required. A solution of the azo compound at a concentration of 1 g/L was prepared in methanol. BSA solution at a concentration of 5 g/L was prepared using water as a solvent. Both solutions were kept for 24 h for homogeneous dissolution. These homogeneously mixed solutions were spread drop-by-drop all over the trough between the two movable surface barriers using a Hamilton syringe (precision of 2.5 μL). Isotherm measurements were started after stabilization of surface pressure at a fixed temperature of 20 °C. All isotherms were recorded at a
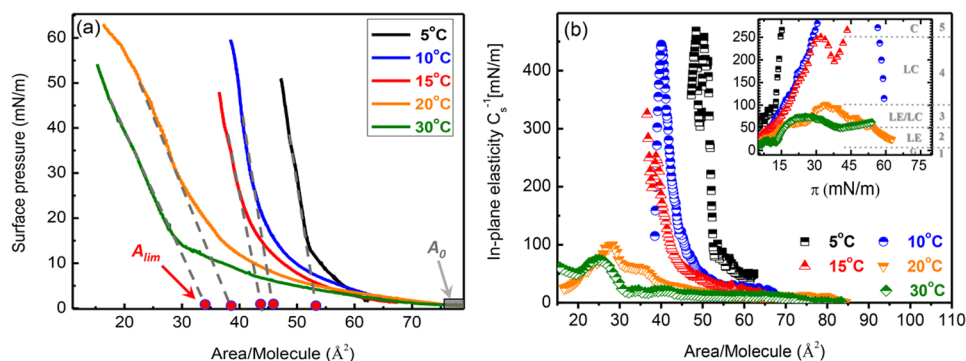
Figure 1. (a) Surface pressure (π)−area/molecule (A) isotherm of 3-Pyab molecules as a function of temperature $(T$ varies from 5 to 30 °C). Dashed line extrapolated to zero pressure axis represents A_{lim}; shaded box represents the A_0 values. These isotherms were collected at fixed pH of Milli-Q water (pH ≈ 6.0). (b) Corresponding in-plane elasticity. Inset, C_s^{-1} vs π curves. Based on C_s^{-1} values molecular assembly can be separated (indicated by horizontal dashed line) into five regimes; regimes 1, 2, 3, 4, and 5 correspond to G, LE, LE/LC, LC, and C phases, respectively.

constant compression speed of 10 mm/min. An isotherm was recorded until the surface pressure attained its maximum value. The temperature of the subphase water was varied from 30 to 5 °C using a chiller (First Source Company). The pH of the subphase was varied using hydrochloric acid and sodium phosphate solution. LB films were deposited at constant pressure π = 30 mN/m onto RCA- and HF-treated Si(100) substrates in one, two, and three strokes. For comparison, some pure azo films were deposited at low surface pressure π = 5 mN/m on both types of Si surfaces. All of the films were deposited maintaining a constant barrier compression speed and expansion speed of 8 mm/min. The lifting and dipping speed of substrates for LB deposition was maintained at 5 mm/min. After deposition, the films were kept for 10 min above the subphase for drying before collecting them. The values of transfer ratio (TR) in the first stroke for all film deposition lay between 0.85 and 0.92, whereas in the subsequent deposition, TR values decreased to 0.4. Additionally, we also prepared pure azo films using the spin-coating technique (Apex Instruments, model EZspinA1) and compared them with the films prepared by LB technique.

XRR measurements were carried out at the MCX beamline[41] of Elettra - Sincrotrone Trieste. The wavelength used was 1.54 Å. The beamline is equipped with a high-resolution four-circle diffractometer and a three dimension $(X, Y,$ and $Z)$ translational stage. Scattered intensities were recorded using a scintillator detector behind a set of receiving slits. Data were taken in specular condition, that is, the incident angle is equal to the reflected angle and both are in a scattering plane. Under such conditions, a nonvanishing wave vector component, $q_z,$ is given by $(4\pi/\lambda)\sin\theta$ with a resolution of 0.0010 Å^{-1}. XRR technique essentially provides an electron density profile (EDP), that is, in-plane $(x-y)$ average electron density (ρ) as a function of depth (z) in high resolution.[42] From EDP, it is possible to estimate film thickness, electron density, and interfacial roughness.[42−44] Analysis of XRR data is carried out using the REFLEX software.[45] In general, the electron-density variation in a specimen is determined by assuming a model and comparing the simulated profile with the experimental data. EDP is extracted from fitting of the experimental XRR data. For the analysis, each film is divided into several layers including roughness at each interface.[42−44] An instrumental resolution in the form of a Gaussian function and a constant background were also included at the time of data analysis. The structural modification of pure azo assembly along the

out-of-plane direction due to the addition of BSA and changing various subphase parameters can be monitored by comparing EDPs of the deposited films.

Surface morphology of the films was collected with an AFM (NT-MDT), and scans were performed over several portions of the films for different scan areas after completion of XRR measurements. AFM images were collected in noncontact mode using a silicon cantilever (dimensions 125 μm × 30 μm, spring constant = 42 N/m, resonance frequency = 320 kHz) and a sharp needle-like tip in ambient conditions to minimize the tip-induced modification of the sample surface. Gwyddion software was used for image processing and analysis.

■ RESULTS AND DISCUSSION

Characteristics of Monolayers at the Air−Water Interface. *Surface Pressure−Area/Molecule Isotherm of Pure 3-Pyab Monolayer: Role of Subphase Temperature.* Figure 1 illustrates the surface pressure (π)−area/molecule (A) isotherms of the pure 3-Pyab compound as a function of temperature. Appreciable differences in the isotherm's characteristics are noticed when the temperature is varied from 5 to 30 °C. The curves shift toward lower area/molecule. From these isotherms, the following parameters can be calculated: limiting area (A_{lim}), lift-off area (A_0), and in-plane elasticity (C_s^{-1}). The limiting area/molecule (A_{lim}), which determines the area/molecule in a closely packed monolayer assembly, is obtained by extrapolating the slope of the compact state to the zero surface pressure axis (shown by dashed lines that intersect the π = 0 axis in Figure 1a, intersection points are indicated by red dots). The calculated values (tabulated in Table 1) of A_{lim} are 54, 46, 44, 38, and 35 Å^2 at T = 5, 10, 15, 20, and 30 °C, respectively. But the value of their corresponding condensation threshold area or lift-off area (A_0), which defines the area/molecule at which the transition from the gas phase to liquid expanded phase occurs and the isotherm starts to rise from zero pressure (indicated by the gray-colored rectangular box in Figure 1a), exhibits nearly the same value, which lies between 76 and 80 Å^2. Different slopes in each isotherm curve correspond to different physical states that change during compression.[46] A particular state portrays the specific alignment and packing of the floating monolayer.

When the molecules reside far from each other after the solution is spread on the subphase, this phase is known as gas phase (G). As the molecules come closer during compression, they start interacting and causing a rise in surface pressure.

Table 1. Parameters (Peak Value of 2D Elasticity (C_s^{-1}), Limiting Area (A_{lim}), Lift-Off Area (A_0)) Obtained from π–A Isotherms Recorded at Various Temperatures and pH Values[a]

	subphase	C_s^{-1} (mN/m)	A_{lim} (Å^2)	A_0 (Å^2)	phase
T (°C)	5	467	54	76–80	C
	10	443	46		C
	15	326	44		C
	20	101	38		LC
	30	76	35		LC+LE
pH	1	287	50	67	C
	3	216	47	82	LC
	6	133	43	82	LC
	9	45	41	82	LE

[a]From the peak value of C_s^{-1}, the phase of the monolayer during height compression is determined.

This suggests a phase transition from the gas phase to the liquid expanded phase (LE). Further compression leads to liquid condensed phase (LC), followed by solid condensed phase (C).

The in-plane (2-dimensional) static elasticity or compressional modulus (C_s^{-1}) can be calculated from the π–A isotherms using the following equation:[47]

$$C_s^{-1} = -A\left(\frac{d\pi}{dA}\right)_T \tag{1}$$

where A is the area/molecule at a certain surface pressure π. In-plane elasticity represents the steepness of the isotherm curves and reveals variations in the physical state of monolayers and helps to understand the molecular arrangement. According to Davies and Rideal,[48] the gas (G), liquid expanded (LE), liquid expanded/liquid condensed coexistence (LE/LC), liquid condensed (LC), and condensed (C) phases exhibit C_s^{-1} values <12.5, 12.5–50, 50–100, 100–250, > 250 mN/m, respectively. These five regimes, labeled as 1, 2, 3, 4 and 5, are separated by dashed lines as illustrated in the C_s^{-1} vs π plots given in the inset of Figure 1b. Now in our study, the peak values of C_s^{-1} (given in Table 1) are 467, 443, 326, 101, and 76 mN/m at T = 5, 10, 15, 20, and 30 °C, respectively. So, the reduction of temperature leads to higher C_s^{-1} values. Based on the calculated values of C_s^{-1} comparing with those of various phases, it can be inferred that the 3-Pyab monolayer exhibits solid condensed phase (C) at low temperatures, that is, at T = 5, 10, and 15 °C. At relatively higher temperatures, that is, at T = 20 and 30 °C, the same assembly displays liquid condensed (LC) and LC/LE coexisting phases, respectively. This indicates that the interaction among 3-Pyab molecules gets stronger with the reduction of temperature resulting in a rigid and compact monolayer.

To eradicate any kind of uncertainty (if any) in the results obtained from the previous temperature-dependent isotherm experiments, an additional experiment was performed. In this single experiment, the starting surface pressure (π) (i.e., after spreading of the solution followed by stabilization of surface pressure at 1.6 mN/m) of the 3-Pyab molecular assembly was monitored with changing subphase temperature from 5 to 30 °C without moving the barrier (shown in Figure 2). The surface pressure was found to decrease gradually with the rise of temperature. Interestingly, the evolution of limiting area/molecule, A_{lim}, with temperature, obtained from the isotherm experiments, follows a similar trend. So, the reduction of
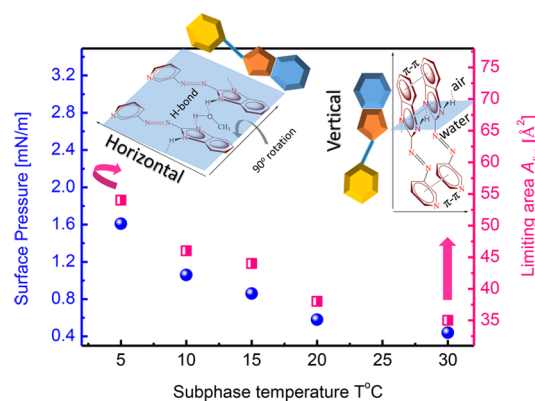

Figure 2. Surface pressure evolution with temperature keeping the barriers in the fully expanded state. Starting surface pressure (after spreading the solution followed by stabilization) is obtained a value of 1.6 mN/m at T = 5 °C. Then we increase the temperature and monitoring the surface pressure at different temperatures. Limiting area (A_{lim}) calculated from the π–A isotherm measurements at those different temperatures is also plotted. Evolution of starting surface pressure resembles the evolution of A_{lim}. Evolution is observed due to the change in the conformation of 3-Pyab molecules (horizontal to vertical, shown schematically in the inset).

surface pressure is accompanied by the reduction of A_{lim} with temperature. This suggests that the conformation changes from horizontal to vertical as the temperature is increased. Pure 3-Pyab molecules dissolved in methanol are arranged horizontally via methanol containing H-bond formation (see the inset of Figure 2). Such bonding is expected to be continued when spread over the LB trough containing water at T = 5 °C. Formation of such a bridging network leads to higher area per molecule (so as A_{lim}) at this low temperature. The occupation of a higher area eventually lowers the surface tension or, in other words, increases the surface pressure. But the gradual increase of subphase temperature breaks these H-bonds, and hence the methanol molecules are dragged into subphase water. Such modifications effectively disturb the molecular association framework and accordingly some molecules change their orientation from horizontal to vertical (90° rotation) as manifested by a lower A_{lim} value. In vertical conformation, the benzene rings of two adjacent 3-Pyab molecules interact through π–π interactions (shown by the dotted line in the inset of Figure 2).

Surface Pressure–Area/Molecule Isotherm of Pure 3-Pyab: Role of Subphase pH. The surface pressure (π)–area/molecule (A) isotherms of the pure 3-Pyab monolayer recorded at four different subphase pHs are depicted in Figure 3a. There is a clear shift of isotherms in the horizontal direction addressing a change in area/molecule. The A_{lim} values are found to be 50, 47, 43, and 41 Å^2 at pH = 1, 3, 6, and 9, respectively, whereas A_0 lies around 82 Å^2 except for that at pH = 1 (given in Table 1). The A_0 is around 67 Å^2 in the latter case. Furthermore, the compressional modulus (C_s^{-1}) was also calculated and is plotted as a function of area/molecule and surface pressure in Figure 3b. The peak values of C_s^{-1} are obtained as 287, 216, 133, and 48 mN/m at pH = 1, 3, 6, and 9, respectively. At pH = 1, the compressed assembly has ended up in the C phase (inset of Figure 3b) above π = 30 mN/m, whereas at pH = 9, the assembly attains LE phase upon maximum compression up to π = 40 mN/m. In
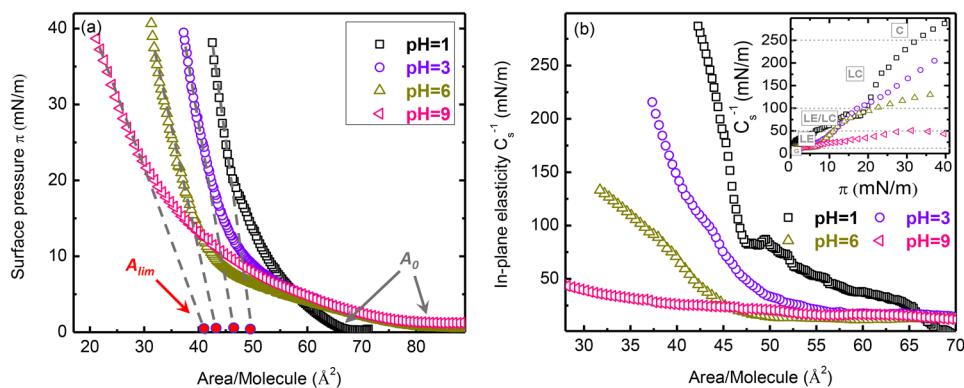
Figure 3. (a) Surface pressure (π)−area/molecule (A) isotherm of the azo compound as a function of pH, (b) corresponding in-plane elasticity. These isotherms were collected at RT. Inset, C_s^{-1} vs π curves. Based on C_s^{-1} values, different phases are marked. Short-dash lines are the boundaries of such different phases.

the intermediate pH values, that is, at 3 and 6, the Langmuir films exhibit LC phase above $\pi = 20$ mN/m.

Initially in the Milli-Q water, the molecules reside at the air−water interface making weak H-bonds between imide (−NH−) hydrogen atoms and the oxygen atoms of methanol (−NH$^{\delta+}\cdots$O$^{\delta-}$−R) and hence dipole−dipole interactions. The addition of HCl into the neutral subphase leads to a reduction of pH from 6 to 1, and accordingly the 3-Pyab molecules capture the H$^+$ ion at the benzimidazole (−NH−C=N−) moiety, which converts to a benzimidazolium ion, that is, −NH$^+$−C=N−).[49] At pH = 1, the molecules exhibit horizontal conformation via strong H-bond interactions between two adjacent molecules keeping methanol at the center. An identical situation was found at the lowest temperature, 5 °C, but the strength of the H-bond is to some extent low. Because molecular force of interaction is higher at pH = 1 compared to that at 5 °C resulting in strong H-bonding between the positive charge (H$^+$) of benzimidazolium ion and the oxygen of methanol (strong ion−dipole interaction). This strong bonding leads to a closed-packed structure of the molecular assembly, and consequently, the A_{lim} value is found to be a little bit smaller at pH = 1 than at the lowest temperature. At pH = 9, the conformation of 3-Pyab molecules is changed from horizontal to vertical because here the interaction is opposite in nature. At high pH, the basic 3-Pyab molecule cannot form H-bonds with the methanol molecule, which primarily resides at the air−water interface. The high concentration of hydroxyl ions in subphase water pulls the imidazole within the water. Hence, the molecules flip from horizontal to vertical conformation resulting in a strong π-π interaction between each benzene and the pyridine ring of the adjacent 3-Pyab molecule, and accordingly, the value of A_{lim} is found to be lowest at pH = 9. Hence the hydrophilic parts feel much more interaction with the subphase water. As a result, azo molecules are dragged into subphase water. Conformational change from horizontal to vertical is induced by changing the pH of the medium. At pH = 1 and 3, the molecules reside horizontally at the air−water interface, but the strength of this interaction decreases with the rise in pH of the medium. Above pH = 3, that is, at pH = 6, some of the molecules may still reside at the air−water interface in horizontal conformation via weak ion−dipole interaction with methanol along with vertically oriented molecules through strong π−π interactions. At low pH, the concentration of H$^+$ ion in water is high; therefore the ionic strength of the

medium is also high. The azo-compound, which is basic in nature due to the presence of the −NH group in the imidazole moiety, can transform into −NH$_2^+$ by accepting H$^+$ ion. The lowering of pH value promotes the formation of −NH$_2^+$ ion, which in turn boosts the ionic strength of the medium.

Compression−Expansion Hysteresis Study. The π−A isotherm curves during compression and decompression (speed remaining constant) may not overlap each other. The term "hysteresis" indicates the deviation of these two curves. There are mainly two reasons that cause hysteresis: (1) conformational change (permanent or temporary) of the molecules under compression or (2) squeezing out of the molecules from the air−water interface (material loss). During compression, an external force in the form of reducing available area is exerted on the molecular assembly to make a closed-packed structure. But in the course of decompression, the external force is removed by providing an available area to attain relaxed organization of the assembly. The basic difference in these two processes is that in the former one the condensed state from the gaseous state is obtained forcefully whereas in the latter case, the condensed film spontaneously chooses a path to reach its original gas state depending on its inherent properties (including cohesion forces between film molecules). Hence hysteresis study is important in elucidating the respreading characteristics of the compressed Langmuir films. Figure 4 depicts the hysteretic behavior of the 3-Pyab molecular assembly in two successive compression−expansion cycles. In the first cycle of compression (C1), surface pressure begins to increase rapidly once the area/molecule goes down to 42 Å^2 (above $\pi = 8$ mN/m) and pressure rises to 40 mN/m. When this compressed assembly is expanded during the expansion cycle (E1), a sudden pressure drop to 4 mN/m ($A \leq 37$ Å^2) followed by a gentle drop to zero is encountered. The hysteresis loop recorded in the second cycle (C2 and E2) does not exhibit overall shift in the vertical and horizontal directions; rather their intermediate trajectories differ in two consecutive compression−expansion cycles. This indicates that in each subsequent cycle an additional modification takes place in the monolayer and the monolayer has yet to reach a stable equilibrium state. Furthermore, as the same surface pressure (40 mN/m) is achieved by the same amount of compression during two subsequent compression cycles (as same minimum area/molecule = 31 Å^2 is obtained for 2 cycles of compression and expansion), the observed hysteresis can be ascribed to the
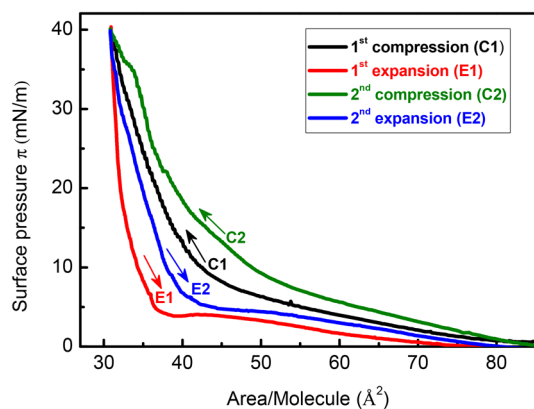
Figure 4. Two-cycle hysteresis study (compression−expansion of two cycles) of the 3-Pyab monolayer at 20 °C, pH = 6. C1 and E1 represent 1st cycle compression and expansion, respectively. C2 and E2 represent 2nd cycle compression and expansion, respectively.

conformation change or reorientation of the molecules at the interface.

Although it is possible that the molecules are squeezed out from the interface along with conformational change during the compression, in the case of squeezing out one can expect a horizontal (change in area/molecule) shift or a vertical (change in surface pressure) shift of the hysteresis loops. However, the hysteresis study is extended in three other pH conditions, at pH = 1, 3, 9, other than pH = 6 as shown in Figure 5. It is evident from this figure that the hysteretic
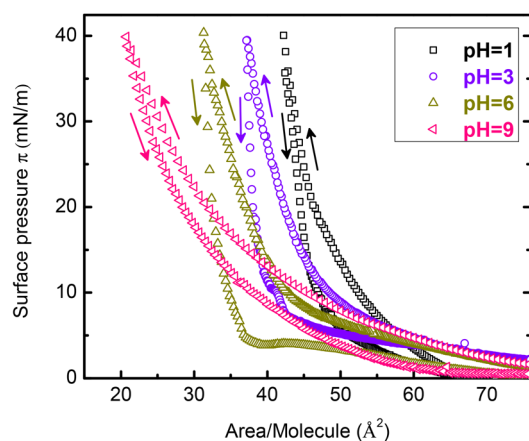

Figure 5. Hysteresis study (compression−decompression) of the 3-Pyab molecule at room temperature with varying pH of subphase water. The direction of arrows indicates the compression and expansion cycles.

property strongly depends on the subphase pH, because at pH = 6 the interaction between the solvent (methanol) and the solute (3-Pyab) is weak at the air−water interface and as a result, the molecules can move from their position to the interior of the water by flipping their conformation from horizontal to vertical.

To understand the hysteric behavior quantitatively the hysteresis area (HA) is calculated using the following equation:[50]

$$
\mathrm{HA} = \left[\left(\int_{A_{\min}}^{A_{\max}} \pi \, \mathrm{d}A \right)_{\mathrm{com}} - \left(\int_{A_{\min}}^{A_{\max}} \pi \, \mathrm{d}A \right)_{\mathrm{exp}} \right]_{n\mathrm{th\text{-}cycle}} \quad (2)
$$

and the normalized value of HA is expressed as

$$
[\mathrm{HA}]_n = \frac{\mathrm{HA}}{A_{\max} - A_{\min}}
$$

The first term in the above equation corresponds to work done per molecule during compression, and the second term corresponds to the same during the expansion cycle. These two terms are nothing but the area under the compression and expansion isotherm curves, respectively. Total work done for compressing 1 mol of molecules is given by[14,51]

$$
W_{\mathrm{com/exp}} = N_a \left(\int_{A_{\min}}^{A_{\max}} \pi \, \mathrm{d}A \right)_{\mathrm{com/exp}} \quad (3)
$$

Hence the difference in work done is

$$
\Delta W = W_{\exp} - W_{\mathrm{com}} \quad (4)
$$

or ΔW can be expressed as

$$
\Delta W = N_a \mathrm{HA} \quad (5)
$$

Since a significant hysteresis associated with the rearrangement of the film-forming molecules is observed, the entropy of the assembly may differ in each cycle. Applying fundamental laws of thermodynamics in this isothermal (T is constant around 20 °C) compression−expansion cycle of a 2D monolayer system, one can calculate the change in entropy using the following equation:[14]

$$
\Delta S = \frac{\Delta W}{T} = \frac{N_a \mathrm{HA}}{T} \quad (6)
$$

Analysis of hysteresis curves in light of eqs 2 and 6 gives the values of HA, $[\mathrm{HA}]_n$, and ΔS, which are tabulated in Table 2. The HA and $[\mathrm{HA}]_n$, and hence ΔS value increase from pH = 1 to pH = 6. Further increase in pH leads to a reduction of these parameters. So hysteresis is found to be more pronounced at pH = 6 and less pronounced at other pH values (i.e., pH = 1, 3,

Table 2. Calculation of Maximum ($A_{\max}$[a]) and Minimum ($A_{\min}$[b]) Area per Molecule, Area under the Isotherm Curves[c] in Compression and Expansion Cycle, Hysteresis Area (HA), Normalized HA ($[\mathrm{HA}]_n$), and Entropy (ΔS)

| pH | cycle | $A_{\max}$ (Å^2) | $A_{\min}$ (Å^2) | area under isotherm curves | | HA (×10^{-22} J) | $[\mathrm{HA}]_n$ (mN/m) | ΔS (J mol^{-1} K^{-1}) |
				compression (×10^{-22} J)	expansion (×10^{-22} J)			
1		71	42	268	160	108	3.7	−22.2
3		75	37	351	215	136	3.6	−27.9
6	1	80	31	402	171	231	4.7	−47.5
6	2	80	31	535	294	241	4.9	−49.5
9		78	21	664	470	194	3.4	−40.0

[a]Equivalent to lift-off area. [b]Slightly less than limiting area/molecule. [c]Area under isotherm curve indicates work done.
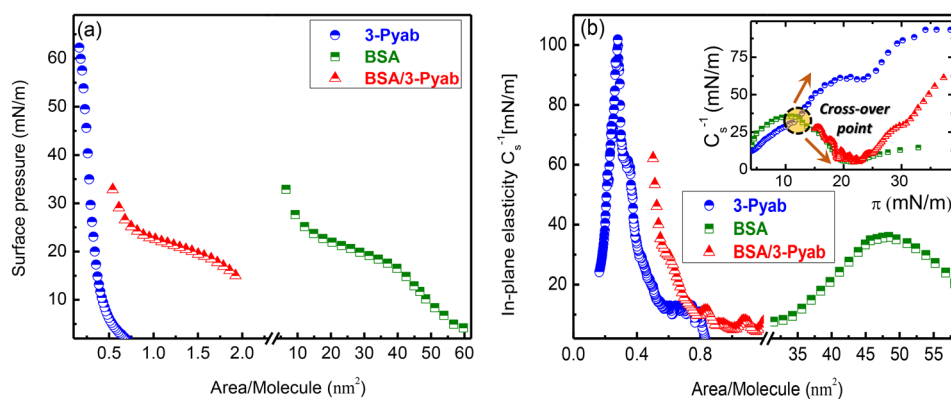
Figure 6. (a) Surface pressure (π)−area/molecule (A) isotherm of BSA, 3-Pyab, and their mixture at RT. (b) Corresponding in-plane elasticity. These isotherms were collected at fixed pH of Milli-Q water (pH ≈ 6.0) at RT. Inset, C_s^{-1} vs π curve. The crossover point of BSA, 3-Pyab, and their mixture is indicated by dashed circle. The dip appearing at π = 22 mN/m is due to the LE−LC phase transition (coexisting phases).

and 9). A negative value of entropy change (ΔS) indicates that the disorder of a system has decreased.[51] In the present work, the molecules constituting an assembly at the air−water interface become more organized in each compression−expansion cycle at a fixed pH and accordingly a more negative ΔS is obtained.

Surface Pressure−Area/Molecule Isotherm of 3-Pyab/BSA Binary Monolayer. Figure 6 shows the $\pi−A$ isotherm of the 3-Pyab/BSA binary monolayer. For comparison, the isotherms of pure 3-Pyab and pure BSA are presented in the same figure. Here BSA molecules were spread on a preformed fully expanded 3-Pyab monolayer. The introduction of a small amount (1.1×10^{-7} mol or mole fraction X_{BSA}= 0.02) of BSA induces drastic changes in the isotherm of the 3-Pyab monolayer, which confirms the adsorption of BSA in the 3-Pyab monolayer. The shape of the isotherm resembles that of pure BSA. Similar changes were reported by de Souza et al.[52] in the phospholipid monolayer due to the incorporation of an ever-smaller amount (10^{-9} mol) of BSA. A large plateau region, suggesting the coexistence of LE and LC phases, appeared in the isotherm of the binary system, which was absent in the pure azo monolayer. Perhaps the interaction between protein and azo molecules brings a phase transition from LE to LC phase upon compression. Furthermore, the isotherm of the hybrid system is shifted toward a higher area due to the mixing of BSA with 3-Pyab. This implies that the BSA molecules are adsorbed within the monolayer assembly of 3-Pyab to make a binary mixed system. The compressional modulus (C_s^{-1}) derived from these isotherms is depicted in Figure 6b. Owing to the inherent structural flexibility of BSA, it exhibits lower C_s^{-1} values (0−36 mN/m). Accordingly, a huge reduction in C_s^{-1} value, from 101 to 62 mN/m, due to the incorporation of BSA in 3-Pyab monolayer matrix is obtained. A deeper look into the C_s^{-1} vs π curves (shown in the inset of Figure 6b) reveals that there is a crossover point (located at π_{cross} = 12.2 mN/m marked by dashed circle) of the elasticity curves of pure 3-Pyab and BSA molecules. Below π_{cross} their deviation or difference is less significant whereas above π_{cross}, they deviate progressively. The elasticity curve of mixed monolayer brings to mind both curves of pure BSA and 3-Pyab. It looks like that of BSA until the pressure reaches a value of 23.8 mN/m, and beyond this, it resembles the wave-like pattern of the 3-Pyab monolayer.

To understand the interaction between constituent molecules within the binary monolayer and its thermodynamic

stability, the surface excess Gibbs energy, ΔG_{exc} is calculated from the deviation of experimental area/molecule (A_{exp}^{mix}) from ideal area/molecule (A_{id}^{mix}) related to an ideal mixture model using the following equations:[47]

$$\Delta G_{exc} = N_a \int_0^\pi A_{exc} \, d\pi \qquad (7)$$

where

$$A_{exc} = A_{exp}^{mix} - A_{id}^{mix}$$

$$A_{id}^{mix} = A_{3\text{-Pyab}}X_{3\text{-Pyab}} + A_{BSA}X_{BSA}$$

Here $A_{3\text{-Pyab}}$ and A_{BSA} are the area/molecule of pure 3-Pyab and pure BSA monolayers at particular surface pressure and $X_{3\text{-Pyab}}$ (0.98) and X_{BSA} (0.02) are their corresponding mole fractions. These different areas, A_{id}^{mix}, A_{exp}^{mix}, and A_{exc}, and the excess Gibb's free energy of mixing, ΔG_{exc}, are plotted in Figure 7 at different surface pressures. The excess area, A_{exc},
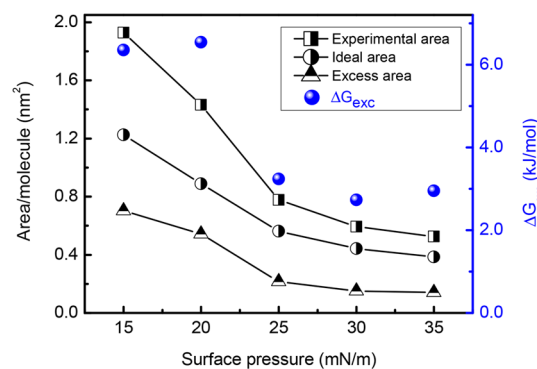

Figure 7. Experimental area, ideal area, and excess area (A) at five different surface pressures the mixture at RT. ΔG_{exc} (blue scale on the right side) is also plotted as a function of surface pressure.

varies from 0.5 to 2.5 nm^2 in the pressure range of 35 to 15 mN/m. It becomes less pronounced at higher pressure. The value of A_{exc} measures the deviation of the experimentally measured area (A_{exp}^{mix}) from the theoretically calculated area (A_{id}^{mix}) of the binary monolayer. If BSA molecules are mixed perfectly with 3-Pyab molecules, then the value of A_{exc} will be zero because the A_{exp}^{mix} value coincides with A_{id}^{mix}. In practice, the interaction between these two constituent molecules leads to a
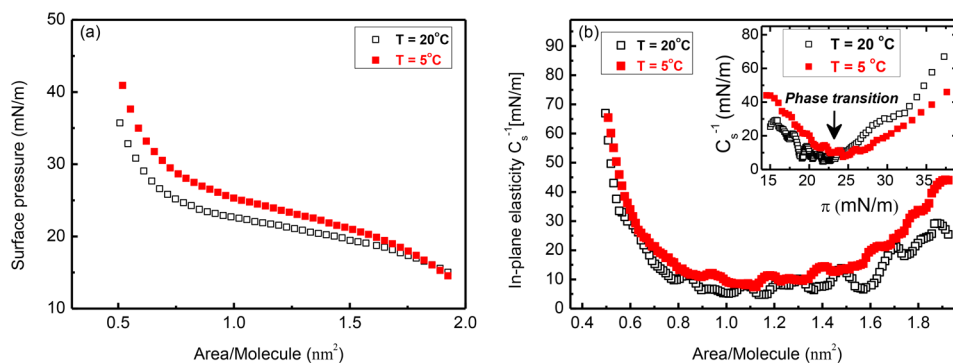
Figure 8. (a) Surface pressure (π)−area/molecule (A) isotherm of 3-Pyab/BSA mixture at T = 20 and 5 °C. (b) Corresponding in-plane elasticity. These isotherms were collected at fixed pH of Milli-Q water (pH ≈ 6.0). Inset, C_s^{-1} vs π curve. The minimum indicated by an arrow corresponds to the LE−LC phase transition (coexisting phases).
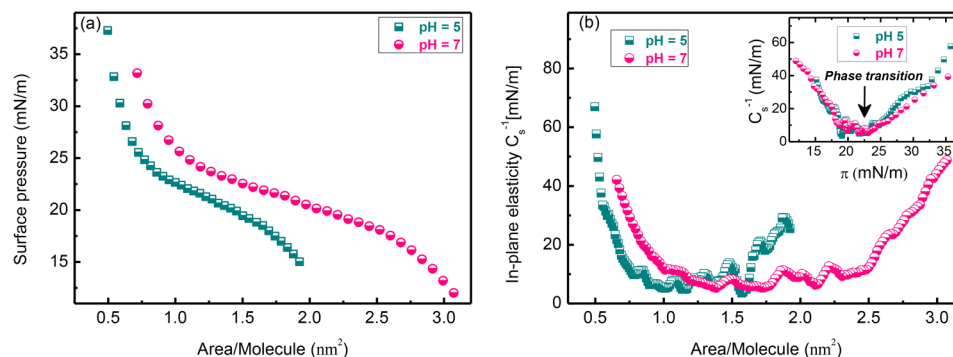

Figure 9. (a) Surface pressure (π)−area/molecule (A) isotherm of 3-Pyab/BSA mixture at pH = 5 and 7. These isotherms were collected at RT. (b) Corresponding in-plane elasticity (C_s^{-1}). Inset, C_s^{-1} vs π curve. The minimum indicated by an arrow corresponds to the LE−LC phase transition (coexisting phases).

higher A_{exp}^{mix} than A_{id}^{mix}. This interaction is repulsive as $A_{exp}^{mix} > A_{id}^{mix}$. However, the value of ΔG_{exc} varies from 2.7 to 6.5 kJ/mol throughout the measured surface pressures. The positive value of ΔG_{exc} indicates that the mixing process of the constituent monolayers is not thermodynamically favorable as they experience repulsive interactions in the binary monolayer.

The surface pressure (π)−area/molecule (A) isotherm measurements of the binary monolayer were performed at two different temperatures (shown in Figure 8a) and pH values (shown in Figure 9a) of the subphase. There is a subtle change in the π−A isotherm curve with temperature as depicted in Figure 8a, although an appreciable change in the isotherm of the pure 3-Pyab monolayer with temperature (see Figure 1a) was encountered. Thus, the binary monolayer exhibits less temperature-responsive behavior. At a particular pressure, the 3-Pyab/BSA binary monolayer occupies marginally larger areas with the reduction of temperature. A similar trend was also observed in the case of the pure 3-Pyab monolayer (see Figure 1a). There is a very small change in the isotherm with temperature change in the mixed system. This change occurs due to the subtle modification of conformation of 3-Pyab molecules, although in the case of pure 3-Pyab assembly the change in temperature causes a substantial change in the isotherm (see Figure 1a). Pure 3-Pyab molecules exhibit conformational transition from horizontal to vertical with the gradual rise of temperature by breakage of H-bonds made with methanol (see inset of Figure 2). Such flipping leads to lower A_{lim} value. Notably, the effect of temperature seems less substantial in the presence of BSA. The modification of the

conformation is restricted by the absorbed BSA molecules within the 3-Pyab assembly. In-plane elasticity, depicted in Figure 8b, shows a reduced value of ~5−10 mN/m in the center and higher values, ~25−70 mN/m, on either side of area/molecule. The plateau that appears between π = 20−25 mN/m in the π−A isotherm (Figure 8a) can be attributed to the LE−LC phase transition. This transition is better viewed as a dip (minimum) in the C_s^{-1} vs π curve (shown by the arrow in the inset of Figure 8b).

The isotherms of the 3-Pyab/BSA binary monolayer recorded at two different subphase pH = 5 and 7 are shown in Figure 9a. The isotherm shifts toward higher area/molecule at a particular surface pressure or higher surface pressure at a fixed area/molecule. The isoelectric point (pI) of BSA lies between pH = 4.6 and 5.1.[53] So, the net charge of BSA is neutral around the pH = 5, whereas at pH = 7, it becomes negatively charged. BSA can exist in folded and unfolded state at pH 5 and 7, respectively. Therefore, at pH = 5 some cationic form 3-Pyab molecules reside in the pocket of BSA molecules by strong ion−dipole interaction between the benzimidazolium of 3-Pyab and neutral amino acids of BSA molecules, and overall area will be minimum in this situation. Perhaps, the negatively charged BSA molecules exist in unfolded state and interact with neutral 3-Pyab molecules via strong ion−dipole intermolecular interactions, which keeps the overall negative charge around the BSA frame, and they repel each other and manifested in higher molecular areas. Such conformational changes of proteins at the air/water interface are the subject of many studies.[54]
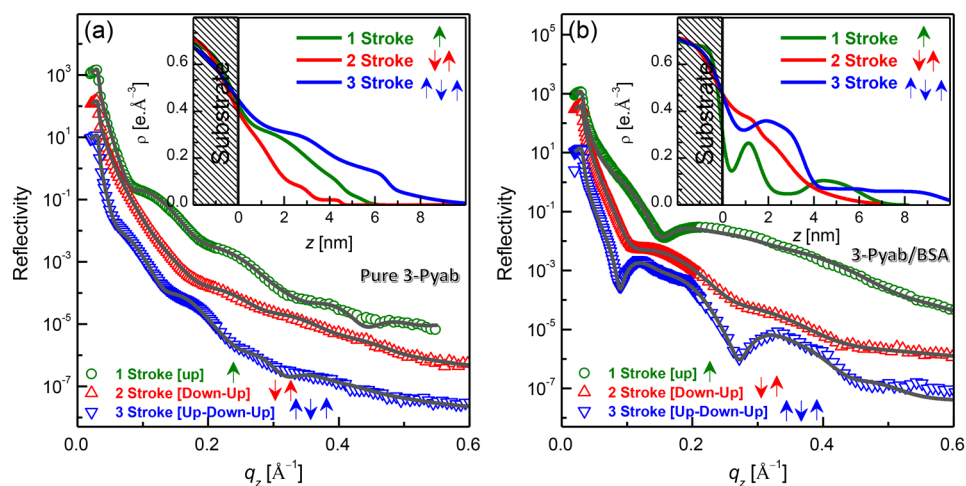
Figure 10. XRR data (different symbols) and analyzed curves (solid line) of (a) pure 3-Pyab and (b) 3-Pyab/BSA LB films on hydrophilic (1 stroke [up] and 3 stroke [up−down−up]) and hydrophobic (2 stroke [down−up]) Si(100) substrates, deposited at surface pressure π = 30 mN/m, pH = 5, and T = 20 °C (curves are shifted vertically for clarity). Inset, corresponding EDPs. The substrate−film interface position is labeled as z = 0 nm.

Structure of Pure and Binary LB Films on the Si Surface. The structural characterization is easier in the case of solid-supported LB films than that of Langmuir films.[14] Thus, a good alternative to in situ characterization of Langmuir monolayer in a LB trough is to imitate the assembly on the substrate using LB deposition.[46,55] Monolayer (upstroke), bilayer (downstroke−upstroke), and trilayer (upstroke−down-stroke−upstroke) depositions of floating molecules were chosen for the preparation of LB films on desired Si surfaces at surface pressure π = 30 mN/m. Nevertheless, for monolayer (1s) and trilayer (3s) depositions, hydrophilic native-oxide covered Si surfaces were used, whereas for bilayer (2s) deposition hydrophobic oxide-free H-passivated Si was used. The structure of LB films, extracted from XRR analysis (out-of-plane structure) and AFM (lateral structure of top surface), can be correlated with the packing, conformation, and organization of pure and mixed molecules in the Langmuir monolayer at the air−water interface. The structural modifications of 3-Pyab and 3-Pyab/BSA binary Langmuir monolayers caused by three factors, (1) incorporation of BSA, (2) subphase temperature, and (3) subphase pH, can be realized after relocating them onto solid substrates (e.g., Si) followed by characterization using XRR and AFM techniques. In the following section, these factors will be discussed in detail.

Structure of LB Films on Si Surface. *X-ray Reflectivity and Electron Density Profile. Structural Modification of 3-Pyab LB Films due to BSA Insertion.* To know the role of BSA in the structural modification of 3-Pyab/BSA binary LB films, XRR measurements were performed on both types of films, pure 3-Pyab (Figure 10a) and 3-Pyab/BSA mixed (Figure 10b) LB films prepared in 1s, 2s, and 3s at a particular pressure π = 30 mN/m. Other parameters, such as T and pH, are kept at 20 °C and 5, respectively. Films prepared at π = 5 mN/m reveal low coverage and are less organized compared to those at π = 30 mN/m (see Supporting Information S1). A pressure of 30 mN/m was chosen because at this pressure all floating monolayers attain a compact structure and hence the quality of LB films is expected to be the best one along with a higher TR value (~0.92). Qualitative differences between 3-Pyab and 3-Pyab/BSA LB films are evident in the XRR curves (Figure

10). To determine the quantitative difference, the simulated EDP is extracted and given in the inset of Figure 10a,b. Before that, the differences within the pure 3-Pyab or 3-Pyab/BSA films prepared in a different number of strokes need to be explored. The EDP of 3s azo films shows a distinct 3-layer structure where the electron densities of the successive layers decay from the bottom (attached to the substrate interface) (~0.315 e·Å^{-3}) to the top (~0.033 e·Å^{-3}) of the film. The density of the intermediate layer is ~0.153 e·Å^{-3}. Such layering is less pronounced in the 1s film, although the density of the bottom layer is nearly the same as that of the 3s film. In the case of 2s pure azo film, the density is found to be lower suggesting a low covered film. Owing to the dominant polar nature of the 3-Pyab molecule, the deposition on the hydrophobic Si substrate in 2s is to some extent prohibited. The total thickness of 1s, 2s, and 3s films is 5.0, 4.3, and 8.0 nm, respectively. Considering a 3-layer structure in the 3s film, which has a thickness of 8.0 nm, each layer has a thickness of 2.6 nm (approx.). The theoretically calculated length of one 3-Pyab molecule is ~1.8 nm. The greater thickness (2.6 − 1.8 = 0.8 nm) of the individual layers obtained from the EDP can be attributed to the vertical fluctuation of the deposited azo molecules forming a single layer. Hence, the width of each layer is enhanced by compensating its electron density or in-plane coverage. The bilayer formation of 1s (one upstroke) film can be understood considering the transfer of azo molecules during relocation on the substrate followed by their flipping on the top of the adjacent molecules. Moreover, the structure of pure 3-Pyab films is altered significantly when we use a spin coater to prepare the films [see Supporting Information S2]. Identical repeating oscillations suggesting a uniform monolayer, unlike the LB films, are obtained in the spin-coated films deposited on both hydrophilic and hydrophobic Si surfaces.

The XRR and hence EDP of 3-Pyab/BSA binary films (Figure 10b) are completely different from those of their component molecules (i.e., 3-Pyab). This can be attributed to the incorporation of BSA molecules within the azo monolayer at the air−water interface. The presence of BSA in the Langmuir monolayer leads to an altered structure of the LB films. The humps and density contrast throughout the films as

shown in the EDP of Figure 10b indicate the existence of highly dense BSA molecules in binary LB films. The mass density of BSA is $\rho_m \approx 1.32$ g/mL.[56] From mass density, one can calculate electron density using $\rho_m = 3.085 \times \rho$,[57] and we obtained the value of $\rho \approx 0.440$ e·Å^{-3}. Such hump-like modulation was absent in the pure 3-Pyab film EDP. However, the mass density and the electron density of the 3-Pyab molecule are found to be ~0.91 g/mL and ~0.304 e·Å^3, respectively. Surprisingly, at some positions of EDP of 2s and 3s binary films, the density values (~0.362−0.372 e·Å^{-3}) cross the bulk density of the 3-Pyab film. This is only possible if BSA is embedded within the 3-Pyab matrix to form hybrid LB films. On the other hand, the shape of BSA can be considered as oblate having dimensions of 7.8 nm (length) × 7.8 nm (breadth) × 1.8 nm (height).[58] The width of the hump, which is ~2 nm, nearly matches the height of the BSA molecule. Hence the appearance of a hump in a relatively flat background strongly supports the fact that the oblate-shape BSA molecules were transferred onto the Si surface along with 3-Pyab molecules. Accordingly, the thicknesses of binary films in each stroke, 6.5 nm in 1s, 5.4 nm in 2s, and 9.8 nm in 3s, are found to be larger than that of pure 3-Pyab films.

Structural Modification of 3-Pyab/BSA LB Films: Effect of Temperature and pH. To explore the effect of temperature and pH, the LB depositions were also made by reducing the temperature from 20 to 5 °C and increasing the pH from 5 to 7 of subphase water. XRR and EDP of 3-Pyab/BSA hybrid film deposited at low subphase temperature $T = 5$ °C, keeping other parameters fixed, are depicted in Figure 11. For
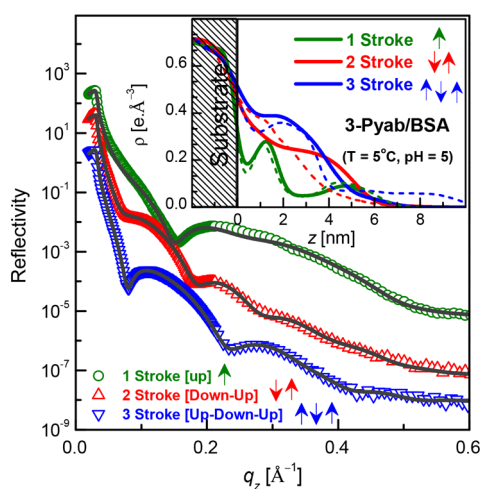

Figure 11. XRR data (different symbols) and analyzed curves (solid line) of 3-Pyab/BSA hybrid LB films on hydrophilic (1 stroke [up] and 3 stroke [up−down−up]) and hydrophobic (2 stroke [down− up]) Si(100) substrates, deposited at $T = 5$ °C, pH = 5, and $\pi = 30$ mN/m (curves are shifted vertically for clarity). Inset, corresponding EDPs shown in solid lines. Dashed lines correspond to the EDPs of the same films (same color) deposited at $T = 20$ °C (already given in Figure 10), plotted again in this figure for comparison. The substrate−film interface position is located at $z = 0$ nm.

comparison, the EDP curves of the films deposited at $T = 20$ °C are also included (as dashed lines in the inset) in this figure. Although the 1s films at these two temperatures look similar, a significant difference is evident in 3s films. The top low-density layer, which was present in the EDP of 3s film deposited at $T = 20$ °C (thickness and density ~6.1 nm and

~0.061 e·Å^{-3}, respectively), is less pronounced at $T = 5$ °C as its density and thickness are ~2.3 nm and ~0.04 e·Å^{-3}, respectively. The 2s film at $T = 5$ °C was found to be thicker and more uniform compared to that at $T = 20$ °C.

XRR and EDP of the 3-Pyab/BSA hybrid film deposited at high pH = 7 keeping the temperature constant at 20 °C are depicted in Figure 12. To visualize the structural modification
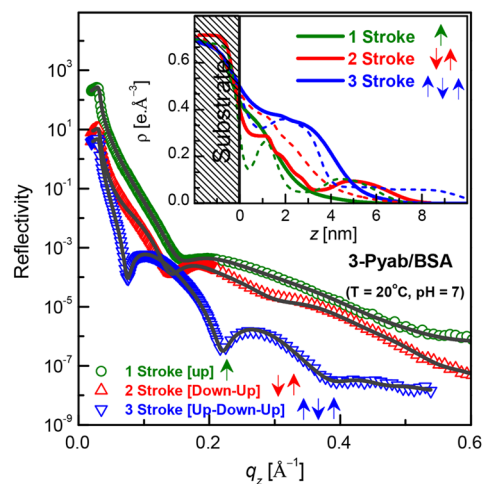

Figure 12. XRR data (different symbols) and analyzed curves (solid line) of 3-Pyab/BSA hybrid LB films on hydrophilic (1 stroke [up] and 3 stroke [up−down−up]) and hydrophobic (2 stroke [down− up]) Si(100) substrates, deposited at pH = 7 (at $\pi = 30$ mN/m and $T = 20$ °C) (curves are shifted vertically for clarity). Inset, corresponding EDPs (solid lines). Dashed lines correspond to EDPs of the same films (same color) prepared at pH = 5. The substrate−film interface position is labeled as $z = 0$ nm.

due to pH change, the EDP curves of similar samples (same substrate surface and the same number of strokes) prepared at pH = 5 are also included as dashed lines in this figure along with high pH samples. Modulation of XRR curves of 1s and 3s films and their EDPs illustrate that the increase in pH up to 7 leads to a structure where the top low-density layer almost vanishes resulting in a uniformly dense film with higher top surface roughness. The XRR curves of 1s and especially of 3s look similar to that of a monolayer film, which was not the case at pH = 5. In contrast, the 2s film on hydrophobic Si exhibits a double-layer structure at pH = 7. The overall film thicknesses of 1s, 2s, and 3s films at pH = 7 are ~4.4, 6.0, and 7.0 nm, respectively. Interestingly, the film thickness on hydrophilic Si (i.e., 1s and 3s films) decreases and that on hydrophobic Si (i.e., 2s film) increases when the pH of the subphase rises from 5 to 7.

Atomic Force Microscopy and Morphology. After XRR measurements, all films were characterized in AFM to extract the surface topography and morphology and correlate with the XRR findings. All the AFM images are depicted in Figure 13. The layered structure of pure 3-Pyab LB films on hydrophilic Si deposited in 1s and 3s is evident from AFM images. Flat domain-like features corresponding to particular layers can be seen. On the other hand, a featureless morphology is exhibited by the 2s LB film of pure 3-Pyab.

The morphology is significantly altered in the case of binary films. Such alteration is more evident in the small area scan (scan area 1000 × 1000 nm^2, see Supporting Information S3). This alteration can be attributed to the BSA insertion within
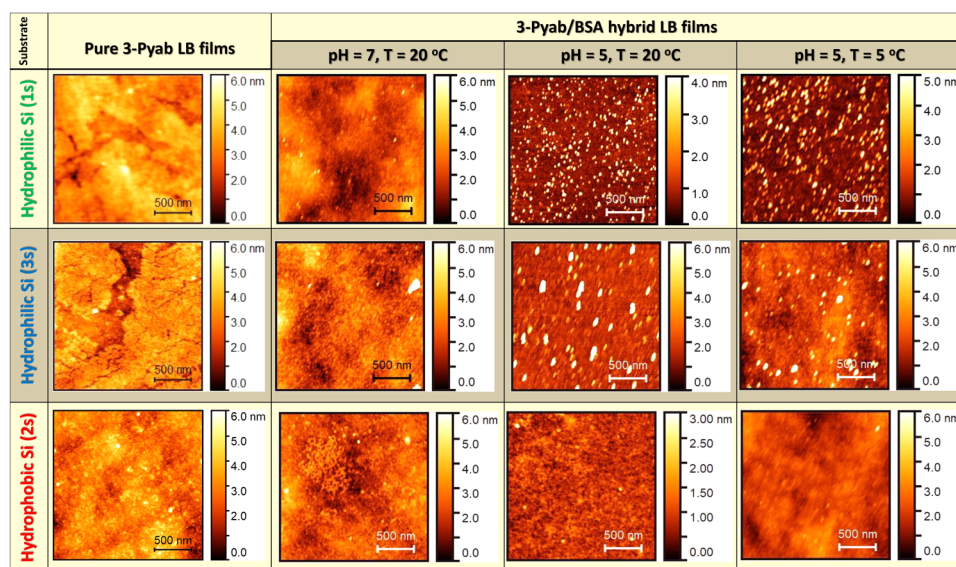
Figure 13. AFM images (scan area = 2000 × 2000 nm²) of pure 3-Pyab and 3-Pyab/BSA binary LB films deposited on hydrophilic and hydrophobic Si(100) substrates by 1, 2, and 3 strokes at π = 30 mN/m varying subphase temperature and pH. Cray scales are given adjacent to the images.
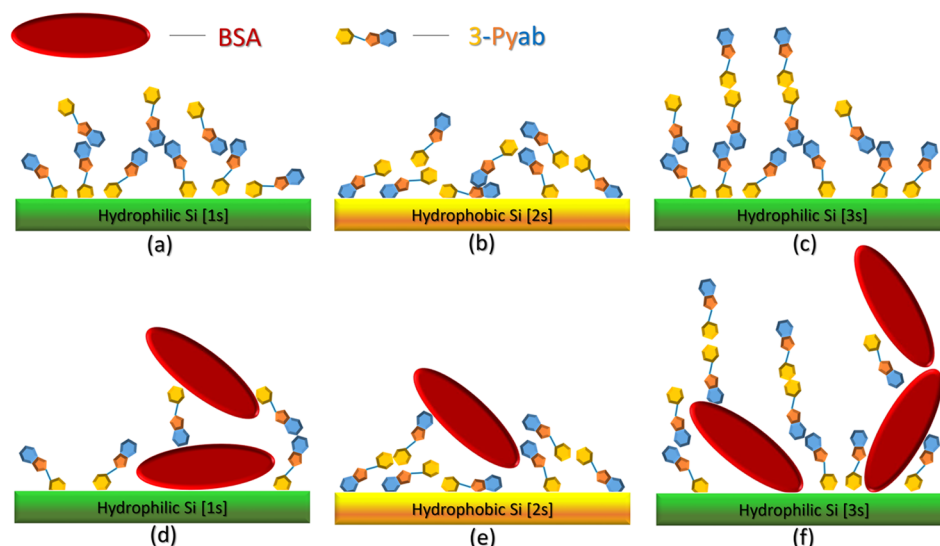

Figure 14. Schematic illustration of pure 3-Pyab (a, b, c) and 3-Pyab/BSA binary (d, e, f) LB films deposited on hydrophilic and hydrophobic Si(100) substrates by 1, 2, and 3 strokes at π = 30 mN/m.

the pure azo matrix. Instead of flat domain-like features, small-sized islands are scattered on top of compact underneath layers. The coverage and size of the islands strongly depend on the temperature and pH of the subphase during film deposition. Height and coverage obtained from AFM are in good agreement with the thicknesses and electron densities of the films measured by XRR. AFM images illustrate that the number density (equivalent to coverage) of the top island-like features is found to be maximum in the 3s LB film deposited at T = 20 °C and pH = 5. The increase of pH up to 7 leads to a substantial reduction of the number density of islands whereas the decrease in temperature to 5 °C makes a small impact on the number density. This outcome was already obtained from XRR analysis. The model structure of the pure 3-Pyab and the binary films extracted from XRR and AFM analysis is schematically depicted in Figure 14.

■ CONCLUSION

In conclusion, the elastic, thermodynamic, and hysteresis properties of a pure aromatic heterocyclic azo compound (3-Pyab) and its mixture with BSA are determined at the air−water interface while varying subphase pH and temperature. Their structures and properties are altered due to the modification of pH and temperature of subphase water. Absorption of BSA within the 3-Pyab matrix strongly modulates those properties. The surface activity and elasticity of pure 3-Pyab are found to decrease with the increase of temperature and with the decrease of pH. Incorporation of BSA within 3-Pyab assembly diminishes the elasticity substantially. The structure of pure 3-Pyab and 3-Pyab/BSA binary films prepared in single to multiple strokes on hydrophobic and hydrophilic surfaces suggests that the structures differ from each other with the number of layers

and with the nature of substrate surfaces. The interaction of BSA with membrane molecules (lipids) has been studied extensively by different groups;[52,53,59] biologically important heterocyclic azo compounds are not reported yet. Thus, this study has potential significance in the field of pharmaceuticals.

■ ASSOCIATED CONTENT

Ⓢ Supporting Information

The Supporting Information is available free of charge at https://pubs.acs.org/doi/10.1021/acsomega.2c00572.

> XRR and EDP of pure 3-Pyab LB films deposited at $\pi = 5$ mN/m and pure 3-Pyab films prepared by spin-coating and AFM images of pure 3-Pyab and 3-Pyab/BSA mixed LB films with high resolution (PDF)

■ AUTHOR INFORMATION

Corresponding Author

Jayanta Kumar Bal − *Abhedananda Mahavidyalaya, University of Burdwan, Sainthia 731234, India;* ⓞ orcid.org/0000-0002-1814-1018; Email: jayanta.bal@gmail.com

Authors

Nilanjan Das − *Abhedananda Mahavidyalaya, University of Burdwan, Sainthia 731234, India*

Tanmay Mathur − *Abhedananda Mahavidyalaya, University of Burdwan, Sainthia 731234, India*

Jasper R. Plaisier − *Elettra - Sincrotrone Trieste S.C.p.A., Trieste 34149, Italy;* ⓞ orcid.org/0000-0003-1981-1498

Sabu Thomas − *International and Inter University Centre for Nanoscience and Nanotechnology, Mahatma Gandhi University, Kottayam 686560, India*

Complete contact information is available at:
https://pubs.acs.org/10.1021/acsomega.2c00572

Author Contributions

J. K. Bal and N. Das contributed to study design, performed research, and analyzed data. T. Mathur contributed to the synthesis of the azo molecule and understanding the research results. J. R. Plasier contributed to data acquisition and analysis of XRR measurements. S. Thomas contributed to the data interpretation and designed the manuscript presentation. All coauthors reviewed and revised the manuscript.

Notes

The authors declare no competing financial interest.

■ ACKNOWLEDGMENTS

■ REFERENCES

(1) Antoci, V.; Cucu, D.; Zbancioc, G.; Moldoveanu, C.; Mangalagiu, V.; Amariucai-Mantu, D.; Aricu, A.; Mangalagiu, I. I. Bis-(imidazole/benzimidazole)-Pyridine Derivatives: Synthesis, Structure and Antimycobacterial Activity. *Future Med. Chem.* 2020, 12, 207−222.

(2) Mantu, D.; Antoci, V.; Moldoveanu, C.; Zbancioc, G.; Mangalagiu, I. I. Hybrid Imidazole(benzimidazole)/ Pyridine-(quinoline) Derivatives and Evaluation of their Anticancer and Antimycobacterial Activity. *J. Enzyme Inhib. Med. Chem.* 2016, 31, 96−103.

(3) Tahlan, S.; Kumar, S.; Narasimhan, B. Pharmacological Significance of Heterocyclic 1H-benzimidazole Scaffolds: A Review. *BMC Chem.* 2019, 13, 101.

(4) Gaba, M.; Mohan, C. Development of Drugs Based on Imidazole and Benzimidazole Bioactive Heterocycles: Recent and Future Directions. *Med. Chem. Res.* 2016, 25, 173−210.

(5) Chiacchio, M. A.; Iannazzo, D.; Romeo, R.; Giofre, S. V.; Legnani, L. Pyridine and Pyrimidine Derivatives as Privileged Scaffolds in biologically Active Agents. *Curr. Med. Chem.* 2020, 26, 7166−7195.

(6) Zhang, J.; Yan, X.; Tian, Y.; Li, W.; Wang, H.; Li, Q.; Li, Y.; Li, Z.; Wu, T. Synthesis of a New Water Soluble Melatonin Derivative with low Toxicity and strong Effect on Sleep Aid. *ACS Omega* 2020, 5, 6494−6499.

(7) Baluja, S.; Movalia, J. Solubility of Some Novel Cyanopyridine Derivatives. *MOJ. Bioorg. Org. Chem.* 2018, 2, 112−117.

(8) Gomtsyan, A. Heterocycles in Drugs and Drug Discovery. *Chem. Heterocycl. Compd.* 2012, 48, 7−10.

(9) Qi, Y.; Wang, J.; Kou, Y.; Pang, H.; Zhang, S.; Li, N.; Liu, C.; Weng, Z.; Jian, X. Synthesis of an Aromatic N-heterocycle Derived from Biomass and Use as a Polymer Feedback. *Nat. Commun.* 2019, 10, 2107.

(10) Raphael, V. P.; Kakkassery, J. T.; Shanmughan, S. K.; Varghese, S. Interaction of Two Water Soluble Heterocyclic Hydrazones on Copper in Nitric Acid: Electrochemical, Surface Morphological, and Quantum Chemical Investigations. *Int. J. Met.* 2016, 2016, 6509469.

(11) Keerthi Kumar, C. T.; Keshavayya, J.; Rajesh, T. N.; Peethambar, S. K.; Shoukat Ali, A. R. Synthesis, Characterization and Biological Activity of 5-Phenyl-1,3,4-thiadiazole-2-amine Incorporated Azo Dye Derivatives. *Org. Chem. Int.* 2013, 2013, 370626.

(12) Kumar, C. T. K.; Keharayya, J.; Tantry, R.; Peethamber, S. K. Synthesis Characterization and Biological Activity of Heterocyclic Azo Dyes Derived From 2-aminobenzothiazole. *Int. J. Pharm. Pharm. Sci.* 2013, 5 (1), 296−301.

(13) Saeed, A. M.; Al-Neyadi, S. S.; Abdou, I. M. Anticancer Activity of Novel Schiff Bases and Azo Dyes Derived From 3-amino-3-hydroxy-2H-pyrano[3,2-c]quinoline-25(6H)-dione. *Heterocycl. Commun.* 2020, 26, 192−205.

(14) Ahmed, I.; Mathur, T.; Islam, A. K. M. M.; Plaisier, J. R.; Parisse, P.; Thomas, S.; Bal, J. K. Structure and Elastic Properties of an Unsymmetrical Bi-Heterocyclic Azo Compound in the Langmuir Monolayer and Langmuir-Blodgett Film. *ACS Omega* 2020, 5, 21538−21549.

(15) Mathur, T.; Jasimuddin, Sk.; Milton, H.; Woollins, J. D.; Sinha, C. R. First Example of Mixed Azo-heterocycles: Structural studies of Metallo Macrocycles. Ag(I) Versus Tetrahedral Cd(II) Complexes of Pyridyl-Azo-Imidazole. *Inorg. Chim. Acta* 2004, 357, 3503−3509.

(16) Mathur, T.; Seal, M.; Chatterjee, S. N.; Saha, N. C. Antimicrobial Activity of Newly Synthesized and Characterized Mixed Bi-Heterocyclic Azo Compound(3-pyridyl-azo-Benzimidazole). *Heterocycl. Lett.* 2017, 7, 1121−1126.

(17) Kulhanek, J.; Bures, F. Imidazole as a Parent π-Conjugated Back-Bone in Charge-Transfer Chromophores. *Beilstein J. Org. Chem.* 2012, 8, 25−49.

(18) Niluvanji Matada, M.; Jathi, K.; Rangappa, M. M.; Geoffry, K.; Ravi Kumar, S.; Nagarajappa, R. B.; Noor Zahara, F. A New Sulphur Containing Heterocycles Having Azo Linkage: Synthesis, Structural Characterization and Biological Evaluation. *J. King Saud Univ., Sci.* 2020, 32, 3313−3320.

(19) Mohanty, S. K.; Khuntia, A.; Yellasubbaiah, N.; Ayyanna, C.; Sudha, B. N.; Harika, M. S. Design, Synthesis of Novel Azo Derivatives of Benzimidazole as Potent Antibacterial and Anti-Tubercular Agents. *Beni-Suef Univ. J. Basic Appl. Sci.* 2018, 7, 646−651.

(20) Pakeeraiah, K.; Mohanty, S. K.; Eswar, K.; Raju, K. Azo Benzimidazole- A Biologically Active Scaffold. *Int. J. PharmTech Res.* **2020**, *13*, 159–171.

(21) Park, H.; Kim, E.-R.; Kim, D. J.; Lee, H. Synthesis of Metal-Azo Dyes and Their Optical and Thermal Properties as Recording Materials For DVD-R. *Bull. Chem. Soc. Jpn.* **2002**, *75*, 2067–2070.

(22) Praveen, P. A.; Babu, R. R. Evaluation of Non-Linear Optical Properties From Molecular Description Of Benzimidazole Metal Complexes by Principal Component Analysis. *J. Mol. Graphics Modell.* **2019**, *93*, 107447.

(23) Al-Madhagi, L. H.; Callear, S. K.; Schroeder, S. L. M. Hudrophillic and hydrophobic Interactions in Concentrated Aqueous Imidazole solutions: A Neutron Diffraction and Total X-Ray Scattering Study. *Phys. Chem. Chem. Phys.* **2020**, *22*, 5105–5113.

(24) Ahmad, D.; van den Boogaert, I.; Miller, J.; Presswell, R.; Jouhara, H. Hydrophilic and Hydrophobic Materials and Their Application. *Energy Sources, Part A* **2018**, *40*, 2686–2725.

(25) Rafols, C.; Bosch, E.; Ruiz, R.; Box, K.; et al. Acidity and Hydrophobicity of Several New Potential Antitubercular Drugs: Isoniazid and Benzimidazole Derivatives. *J. Chem. Eng. Data* **2012**, *57*, 330–338.

(26) Slassi, S.; Fix-Tailler, A.; Larcher, G.; Amine, A.; El-Ghayoury, A. Imidazole and Azo Based Schiff Bases Ligands as Highly Active Antifungal and Antioxidant Compounds. *Heteroat. Chem.* **2019**, *2019*, 1–8.

(27) Schehr, M.; Ianes, C.; Weisner, J.; Heintze, L.; Muller, M. P.; Pichlo, C.; Charl, J.; Brunstein, E.; Ewert, J.; Lehr, M.; Baumann, U.; Rauh, D.; Knippschild, U.; Peifer, C.; Herges, R. 2-Azo-2-Diazocine-Thiazole and 2-Azo-Imidazoles as Photoswitchable Kinase Inhibitors.: Limitations and Pit Falls of The Photoswitchable Inhibitors Approach. *Photochem. Photobiol. Sci.* **2019**, *18*, 1398–1407.

(28) Mahdi, M. A.; Jasim, L. S.; Mohamed, M. H. Synthesis, Spectral and Biological Studies of Co(II), Ni(II) and Cu(II) Complexes with New Heterocyclic Ligand Derived From Azo-Dye. *Syst. Rev. Pharm.* **2021**, *12*, 426–434.

(29) Hameed, A. N.; Atia, A. J. K.; Al-Sharifi, H. K. R. Synthesis of New Azo-Chalcone Compound Derived from Imidazoleline-4-One and Evaluation Their Biological Activity. *Eur. j. mol. clin. med.* **2020**, *7*, 3565–3589.

(30) Al-Adilee, K. J.; Atyha, S. Synthesis, Spectral, Thermal and Biological Studies of Some Metal Complexes Derived From Heterocyclic Mono-Azo Dye Ligand 2′[2′-Hydroxy-4-methylphenyl)-azo]imidazole. *Asian J. Chem.* **2018**, *30*, 280–292.

(31) Crespi, S.; Simeth, N. A.; Konig, B. Heteroarylazo dyes as Molecular Photoswitches. *Nat. Rev. Chem.* **2019**, *3*, 133–146.

(32) Erbas, S.; Uregil, U.; Gulle, S.; Basturk, S. B. Investigation of Spectroscopic and Thermo-Mechanical Behaviors of Different Phenanthro-imidazole-Azo Dyes in Solvent and Polymer Medium. *Mater. Res. Express* **2020**, *7*, 035101.

(33) Girard-Egrot, A. P.; Godoy; Blum, L. J. Enzyme association with lipidic LangmuirBlodgett films: Interests and applications in Nanobioscience. *Adv. Colloid Interface Sci.* **2005**, *116*, 205–225.

(34) Beigi, F.; Lundahl, P. Immobilized biomembrane chromatography of highly lipophilic Drugs. *J. Chromatogr. A* **1999**, *852*, 313–317.

(35) Okahata, Y.; Tsuruta, T.; Ijiro, K.; Ariga, K. Langmuir-Blodgett Films of an EnzymeLipid Complex for Sensor Membranes. *Langmuir* **1988**, *4*, 1373–1375.

(36) Hou, S.; Wang, J.; Martin, C. R. Template-Synthesized Protein Nanotubes. *Nano Lett.* **2005**, *5*, 231–234.

(37) Siwy, Z.; Trofin, L.; Kohli, P.; Baker, L. A.; Trautmann, C.; Martin, C. R. Protein Biosensors Based on Biofunctionalized Conical Gold Nanotubes. *J. Am. Chem. Soc.* **2005**, *127*, 5000–5001.

(38) Pedraz, P.; Montes, F. J.; Cerro, R. L.; Díaz, M. E. Characterization of Langmuir biofilms built by the biospecific interaction of arachidic acid with bovine serum albumin. *Thin Solid Films* **2012**, *525*, 121–131.

(39) Bal, J. K.; Beuvier, T.; Unni, A. B.; Chavez Panduro, E. A.; Vignaud, G.; Delorme, N.; Chebil, M. S.; Grohens, Y.; Gibaud, A. Stability of polymer ultrathin films (<7 nm) made by a top-down approach. *ACS Nano* **2015**, *9*, 8184–8193.

(40) Bal, J. K.; Kundu, S.; Hazra, S. Hydrophobic to hydrophilic transition of HF-treated Si surface during Langmuir-Blodgett film deposition. *Chem. Phys. Lett.* **2010**, *500*, 90–95.

(41) Rebuffi, L.; Plaisier, J. R.; Abdellatief, M.; Lausi, A.; Scardi, P. MCX: A synchrotron radiation beamline for X-ray diffraction line profile analysis. *Zeitschrift fur Anorg. und Allg. Chemie* **2014**, *640*, 3100–3106.

(42) Daillant, J.; Gibaud, A. *X-ray and Neutron Reflectivity: Principles and Applications*; Springer: Berlin, 1999.

(43) Bal, J. K.; Mukherjee, M.; Delorme, N.; Sanyal, M. K.; Gibaud, A. Concentration mediated structural transition of triblock copolymer ultrathin films. *Langmuir* **2014**, *30*, 5808–5816.

(44) Bal, J. K.; Beuvier, T.; Chebil, M. S.; Vignaud, G.; Grohens, Y.; Sanyal, M. K.; Gibaud, A. Relaxation of ultrathin polystyrene films hyperswollen in supercritical carbon dioxide. *Macromolecules* **2014**, *47* (24), 8738–8747.

(45) Vignaud, G.; Gibaud, A. REFLEX : A Program for the Analysis of Specular X-Ray and Neutron Reflectivity Data. *J. Appl. Crystallogr.* **2019**, *52* (1), 201–213.

(46) Gochev, G. G.; Kovalchuk, V. I.; Kovalchuk; Aksenenko, E. V.; Fainerman, V. B.; Miller, R. β-Lactoglobulin Adsorption Layers at the Water/Air Surface: Adsorption Isotherm and Equation of State Revisited, Impact of pH. *Colloids Interfaces* **2021**, *5*, 14.

(47) Ahmed, I.; Dildar, L.; Haque, A.; Patra, P.; Mukhopadhyay, M.; Hazra, S.; Kulkarni, M.; Thomas, S.; Plaisier, J. R.; Dutta, S. B.; Bal, J. K. Chitosan-Fatty Acid Interaction Mediated Growth of Langmuir Monolayer and Langmuir-Blodgett Films. *J. Colloid Interface Sci.* **2018**, *514*, 433–442.

(48) Davies, J. T.; Rideal, E. K. *Interfacial Phenomena*, 2nd ed.; Academic Press: New York, 1963.

(49) Jerez, G.; Kaufman, G.; Prystai, M.; Schenkeveld, S.; Donkor, K. K. Determination of thermodynamic pKa values of benzimidazole and benzimidazole derivatives by capillary electrophoresis. *J. Sep. Sci.* **2009**, *32*, 1087–1095.

(50) Guzmán, E.; Ferrari, M.; Santini, E.; Liggieri, L.; Ravera, F. Effect of silica nanoparticles on the interfacial properties of a canonical lipid mixture. *Colloids Surf., B* **2015**, *136*, 971–980.

(51) Herskovits, T. T.; Harrington, J. P. Solution Studies of the Nucleic Acid Bases and Related Model Compounds. Solubility in Aqueous Alcohol and Glycol Solutions. *Biochemistry* **1972**, *11* (25), 4800–4811.

(52) de Souza, N. C.; Caetano, W.; Itri, R.; Rodrigues, C. A.; Oliveira, O. N., Jr.; Giacometti, G. A.; Ferreira, M. Interaction of small amounts of bovine serum albumin with phospholipid monolayers investigated by surface pressure and atomic force microscopy. *J. Colloid Interface Sci.* **2006**, *297*, 546–553.

(53) Xu, G.; Hao, C.; Zhang, L.; Sun, R. The interaction between BSA and DOTAP at the air-buffer interface. *Sci. Rep.* **2018**, *8*, 407.

(54) Noskov, B. A. The conformation changes of proteins at the air/water interface is the subject of many studies. *Adv. Colloid Interface Sci.* **2014**, *206*, 222–238.

(55) Ahmed, I.; Haque, A.; Bhattacharyya, S.; Patra, P.; Plaisier, J. R.; Perissinotto, F.; Bal, J. K. Vitamin C/Stearic Acid Hybrid Monolayer Adsorption at Air−Water and Air−Solid Interfaces. *ACS Omega* **2018**, *3* (11), 15789–15798.

(56) Richter, A. G.; Kuzmenko, I. Using in Situ X-ray Reflectivity to Study Protein Adsorption on Hydrophilic and Hydrophobic Surfaces: Benefits and Limitations. *Langmuir* **2013**, *29*, 5167–5180.

(57) Vignaud, G.; S. Chebil, M.; Bal, J. K.; Delorme, N.; Beuvier, T.; Grohens, Y.; Gibaud, A. Densification and Depression in Glass Transition Temperature in Polystyrene Thin Films. *Langmuir* **2014**, *30* (39), 11599–11608.

(58) Kundu, S.; Das, K.; Aswal, V. K. Modification of attractive and repulsive interactions among proteins in solution due to the presence of mono-, di- and tri-valent ions. *Chem. Phys. Lett.* **2013**, *578*, 115–119.

(59) Sah, B. K.; Kundu, S. Behaviour of protein (BSA)-lipid (DMPA) mixed monolayer on the spreading order of the individual component. *Chem. Phys. Lipids* **2019**, *225*, 104810−1−9.